Journal of Magnetic Resonance **148,** 155–164 (2001)
doi:10.1006/jmre.2000.2226, available online at http://www.idealibrary.com on IDEAL®

In Vivo EPR Imaging of the Distribution and Metabolism of Nitroxide Radicals in Human Skin

Guanglong He, Alexandre Samouilov, Periannan Kuppusamy, and Jay L. Zweier

EPR Center and Division of Cardiology, Department of Medicine, The Johns Hopkins University School of Medicine, 5501 Hopkins Bayview Circle, Baltimore, Maryland 21224

Received June 30, 2000; revised September 19, 2000

While altered cellular free radical and redox metabolism are critical factors in many human diseases, it has not been previously possible to both measure and image these processes in humans. The development and application of electron paramagnetic resonance instrumentation capable of *in vivo* spectroscopy and imaging of free radicals in human skin are reported. The instrumentation uses a specially designed topical resonator and a 2.2-GHz microwave bridge. Noninvasive measurements of the distribution and metabolism of the topically applied nitroxide, ^{15}N-perdeuterated tempone (100 mM), in forearm skin were performed. A single broad peak due to the concentrated label at the skin surface was initially observed, followed by a sharp doublet from the diluted label that permeated the skin. The penetration of the label into the skin and its metabolic clearance were modeled using kinetic equations. It was observed that the penetration process from the skin surface into the dermis and subcutaneous regions, as well as its clearance from these regions, could be described by single exponential functions. Phantom imaging experiments using the nitroxide showed that a spatial resolution of up to 50 μm could be achieved. The skin imaging measurements showed two bands in the distribution of the label along the skin depth. The first band appeared in the outer 400 μm of the skin, the epidermis region, whereas the second band was centered at a depth of 1000 μm in the subcutaneous region with a thickness about 400 μm. These two bands decayed and merged into a single band with time. The results are important in the understanding of the permeability and metabolism of free radicals in human skin.

Key Words: **EPR imaging; skin; nitroxide; free radicals; bioreduction; metabolism.**

INTRODUCTION

Alterations in cellular free radical generation and cellular redox metabolism are thought to be of critical importance in the pathogenesis of many human diseases. Therefore, there has been a great need to develop methods suitable for measurement of these processes in humans. Electron paramagnetic resonance (EPR) spectroscopy has been shown to be an effective noninvasive method capable of measuring the spatial distribution and pharmacokinetic decay of free radicals in biological systems including isolated organs and small living animals (*1–5*). Imaging of free radicals, redox metabolism, and oxygen is performed using EPR imaging techniques with magnetic field gradients (*3, 6–9*). Imaging of whole biological objects requires the use of resonators with a large sample volume (>1 cm^3) and low frequency (1.4 GHz or less). On the other hand, topical imaging, where the imaging depth is on the order of only a few millimeters, can be performed at higher frequencies with higher sensitivity and resolution (*10, 11*).

Skin is an ideal target organ for the clinical application of EPR spectroscopy and imaging because of the limited thickness of the skin layers, which in turn facilitates the use of higher frequency microwave fields along with topical resonators and locally applied paramagnetic labels. Alterations in free radical generation and metabolism have been proposed to be of critical importance in the process of skin aging, skin photodamage, and a variety of skin diseases. This has received much attention from the cosmetic industry and the public at large. Traditional methods for studying the properties of skin such as the mechanical measurement of elastic properties lack reproducibility because of their dependence on many uncontrollable factors (*12*). In addition, these past methods provide little, if any, insight into the redox state of the skin. Thus, there has long been a need to develop effective noninvasive and nondestructive methods to characterize the properties and redox state of human skin.

EPR spectroscopy and imaging has been previously applied to study skin cells in culture or skin biopsies using conventional X-band EPR instrumentation (*13–20*). The inability of conventional X-band instrumentation to accommodate *in vivo* systems has limited the application of this technology to the study of *in vivo* properties of skin and prevented application of this powerful technology to important clinical applications. While S-band instrumentation has been previously reported to be suitable for *in vivo* surface EPR spectroscopy of human skin (*11*), it has not been previously possible to perform noninvasive measurement and imaging of the spatial distribution of free radicals and the localized process of radical clearance and metabolism in humans.

Therefore, we developed topical S-band EPR instrumenta-

1090-7807/01 $35.00

tion suitable for noninvasive localized EPR spectroscopy and imaging of human skin. A skin-permeable nitroxide radical probe was used and its metabolism and spatial distribution in the skin were measured. A kinetic model is proposed for the penetration and clearance of this radical in the skin. Different human subjects were found to have different skin permeability and metabolism.

MATERIALS AND METHODS

Chemicals

4-Oxo-2,2,6,6-tetramethylpiperidine-d_{16}-1-^{15}N-1-oxyl (^{15}N-perdeutero tempone, ^{15}N-PDT) (CDN Isotopes, Quebec, Canada) was used as spin probe. The ^{15}N-PDT gives a well-separated doublet EPR spectrum with a hyperfine-coupling constant of 22.5 G. It provides for enhanced sensitivity and a narrower linewidth than nonisotope enriched natural abundance tempone, which is of particular importance for EPR imaging. The nitroxide solution was prepared at 100 mM concentration in deaerated double-distilled water, subaliquoted, and kept frozen until use.

EPR Spectroscopy and Imaging Instrumentation

The EPR spectroscopy and imaging experiments were performed on an S-band spectrometer set up for topical measurements of the skin of human volunteers (Fig. 1A). A specially designed bridged loop–gap surface resonator was built with a loop diameter of 7 mm and a sensitive volume depth of up to 6 mm in the direction perpendicular to the surface of the resonator. The surface resonator has a one-loop two-gap structure inside a cylindrical shield and a working frequency of 2.2 GHz when loaded with the human forearm skin. There is an inductive coupling loop close to the opposite end of the cylindrical loop that pivots to vary the coupling of microwave power to the resonator. The surface resonator was fixed through a support board that was fixed between the pole pieces of the magnet at a vertical position to keep the resonator surface centered at the null gradient position. A specially designed cap was attached to the top of the resonator to fix the position of the sample and loading of the resonator. A detailed description of this resonator design is to be reported separately. Three sets of water-cooled gradient coils were used attached to the magnet pole pieces and powered with a specially constructed power amplifier capable of generating up to 150 G/cm gradient field along x, y, and z for the imaging applications, similar to that reported previously (*21*). Sustained gradients of up to 75 G/cm could be maintained for hours without problems due to heating. Customized computer software capable of performing spectral data acquisition and image reconstruction was used (*21, 22*). To determine the homogeneity of the B_1 field and the sensitive diameter and sensitive depth of the resonator, 3-dimensional EPR imaging of a cylindrical phantom of 1 mM ^{15}N-PDT in aqueous 0.5 N saline was performed. The sensitive diameter and depth, defined as diameter or depth within which the image intensity is >20% of maximum, were 7 and 6 mm, respectively. The image intensity was >80% uniform to a depth of 2 mm.

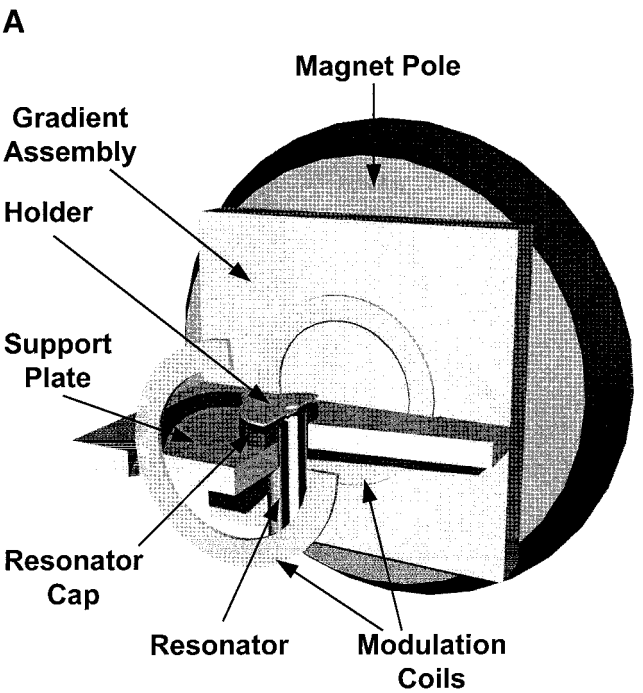

FIG. 1. Experimental setup for topical EPR spectroscopy and imaging of the skin of human volunteers. (A) A sketch of the instrumentation and setup used. The distal magnet pole and gradient set are shown while the proximal magnet pole piece and gradient set are not shown so that the resonator, skin holder, and support plate on which the forearm rests can be seen. The volunteer is seated next to the magnet and extends his/her arm into the magnet gap, resting it on the support plate. The specially designed skin positioning holder is shown in (B). The disk on the bottom of this skin holder locks into a complementary well in the resonator cap precisely fixing the position of the skin with respect to the resonator. (C) A photo of the skin holder attached to the forearm of a human volunteer. Five minutes after nitroxide application, the holder is fixed to the skin with adhesive tapes and the arm is positioned on the support plate such that the holder locks into the resonator cap.

Human Skin Preparation

A human volunteer's forearm skin, about a 6-mm-diameter circular spot, typically at the ulnar surface of the wrist, was washed thoroughly with alcohol and 3.5 μL of 100 mM nitroxide solution (about 2×10^{17} spins) was applied to the marked skin area. Five minutes later, when the deposited solution dried, a specially designed positioning holder with a 7-mm-diameter well and bottom disk that locked into a well in the resonator cap was attached to the skin to fix this region of skin to the surface resonator (Figs. 1B and 1C). EPR and EPRI measurements were then started. Measurements on the volunteers were performed for 15- to 20-min

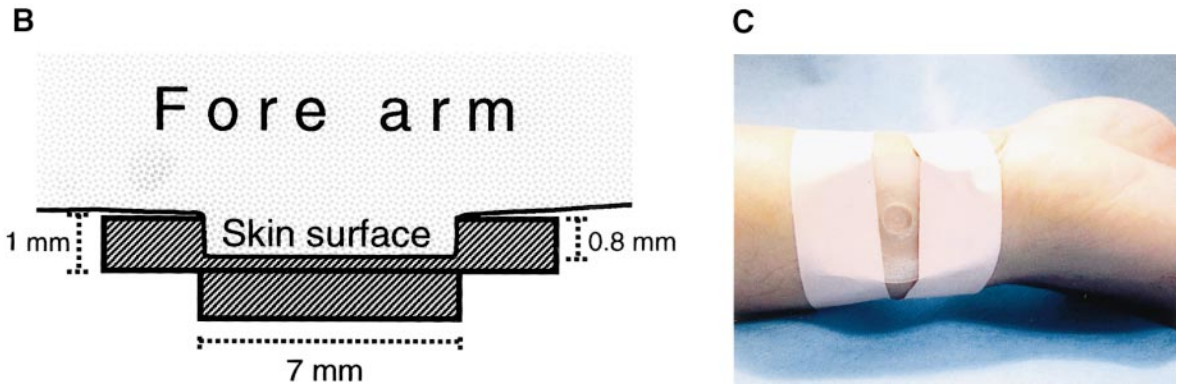

FIG. 1—*Continued*

periods after which there were 30-min rest periods in which the volunteer removed their arm from the resonator and the magnet. The holder fixed the skin positioning and assured a constant filling factor of the loaded resonator. The positioning holder was left attached to the arm for the entire series of measurements, lasting up to 8 h. The preparation of the forearm skin and the dimensions of the spacer are shown in Fig. 1.

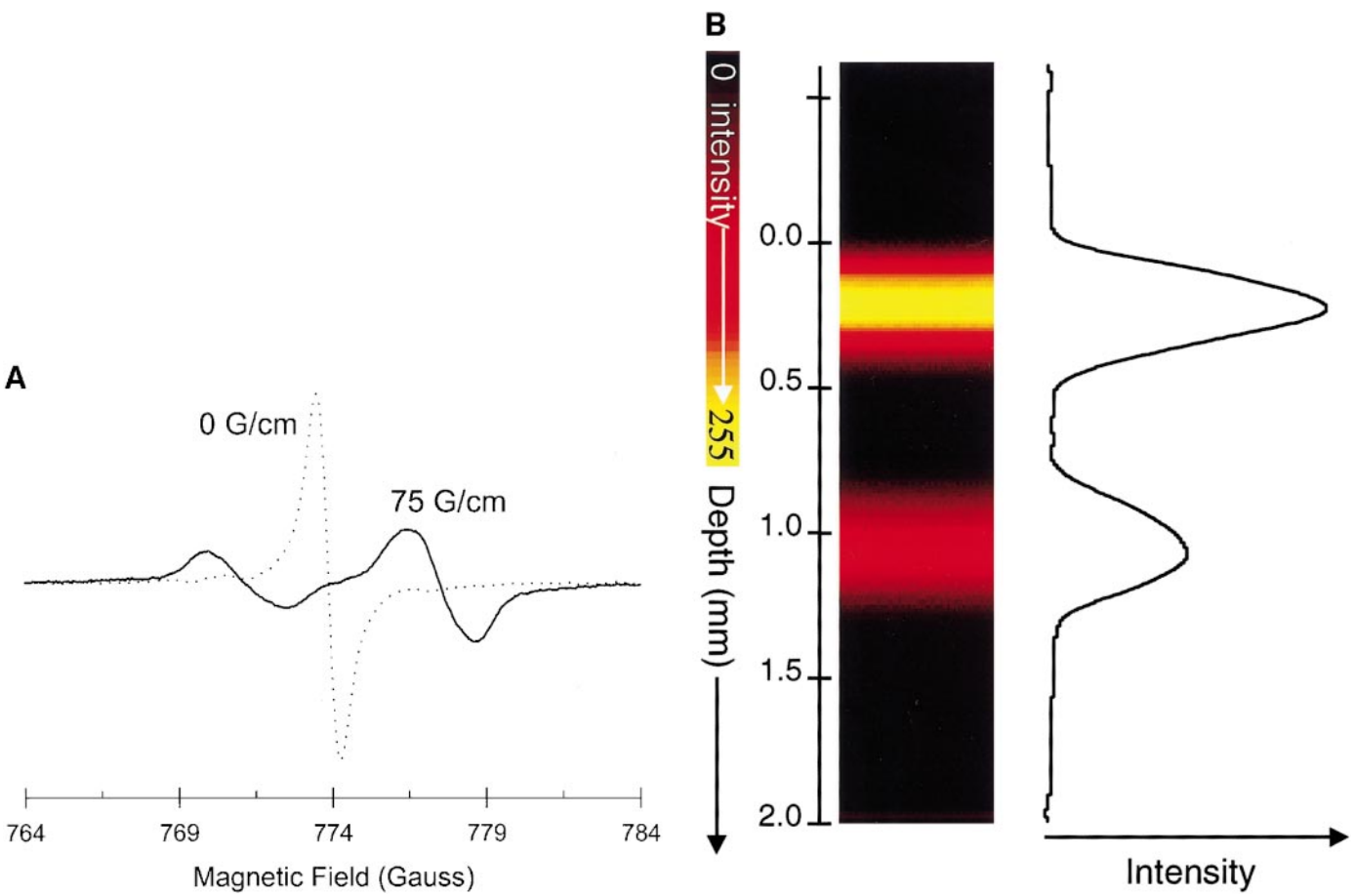

FIG. 2. S-band, 2.2 GHz, EPR spectroscopy and imaging of ^{15}N-PDT in a layered disc phantom. (A) The low-field peak ($m_I = +\frac{1}{2}$) of the nitroxide doublet was scanned in the absence (0 G/cm, dotted line) and presence (75 G/cm, solid line) of field gradient applied normal to the surface of the disc phantom. Data acquisition parameters are given in the text. The splitting observed in the presence of the field gradient is due to the spatial separation of the two discs in the phantom. (B) 1-D spatial image of disc phantom obtained from the projections in (A), shown as a color-coded intensity image or 1-D spatial profile of the nitroxide distribution in the direction perpendicular to the disc face. The data show that a spatial resolution of >100 μm can be obtained.

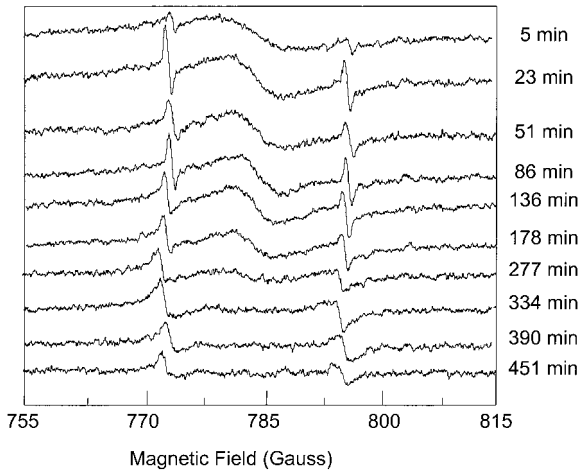

FIG. 3. Time course of the EPR spectra of ^{15}N-PDT applied to human forearm skin. The spectra were obtained at S-band using the topical resonator. A 3.5-μL solution of 100 mM ^{15}N-PDT was applied to the skin and the spectral acquisitions were started 5 min later. Data acquisition parameters are as stated in the text.

RESULTS

Imaging of a Phantom

To validate the measurement range, sensitivity, and resolution of the topical resonator, EPR imaging experiments were performed on a specially constructed phantom. The phantom consisted of two layers of nitroxide solution separated by a thin 200-μm film spacer. The phantom was prepared as follows: two 6-mm-diameter discs of mutilayer tissue paper, thickness approximately 600 μm, were allowed to absorb 5 or 7.5 μL of 5 mM ^{15}N-PDT in water, after which each disk was covered and sealed with self-stick paper tape to the top or the bottom of the 200-μm film spacer.

The EPR spectroscopy and imaging parameters were as follows: frequency, 2.2 GHz; microwave power, 50 mW; modulation amplitude, 0.5 G; scan width, 16 G; scan time, 15 s; time constant, 80 ms; gradient field, 75 G/cm. The spectra of the phantom measured with and without the gradient field are shown in Fig. 2A. A single peak, with a peak–peak width of 0.74 G, was observed in the absence of the field gradient, while a well-resolved profile with two peaks corresponding to the two layers of the nitroxide was observed in the presence of the 75 G/cm field gradient. The nitroxide distribution profile perpendicular to the plane of the layers of the phantom was obtained by 1-D spatial imaging, acquiring spectral projections in the presence and absence of the gradient. Deconvolution was then performed and the resulting profile is the 1-D spatial image (Fig. 2B). The image showed two well-resolved bright bands corresponding to the nitroxide layers. The distance between the two layers of the phantom was accurately measured to be 200 μm. In general, it was observed that a spacing between the layers as small as 50 μm could be resolved.

Penetration, Metabolism, and Spatial Distribution of Nitroxide in Skin

The nitroxide solution was applied to the skin of normal human volunteers at the ulnar surface of the wrist as described above. The holder was attached to the skin and the wrist was placed on top of the resonator with the holder locked into the resonator opening. EPR spectroscopy and imaging measurements were performed as described above. Figure 3 shows the EPR spectra obtained from a volunteer as a function of time. At the beginning, there was a strong and broad signal around the $g \sim 2.00$ region. This broad signal was due to electron spin exchange interaction of the nitroxide radicals in the concentrated solution at the surface of the skin (*23, 24*). With time, the broad central peak gradually became narrower and weaker. In addition, another component with two sharp peaks (doublet) appeared, increased over the first 30 min, and then gradually declined. This component is due to the diluted ^{15}N-PDT within the skin which gives rise to a doublet with hyperfine-coupling constant $a_N = 22.5$ G.

Skin Model and the Kinetics

In order to understand the process of penetration and clearance of the applied nitroxide in the skin, we developed a kinetic model to simulate the time evolution of both the exchange-broadened and the hyperfine doublet components. As can be seen from the time course spectra (Fig. 3), there are two components: a broad singlet from the concentrated nitroxide layer at or near the surface of the skin and a sharp doublet from dilute nitroxide that penetrated into the skin. The penetration of the nitroxide from the skin surface into the skin depletes the radical concentration on top of the skin. The emergence of the sharp doublet component is due to dilution of the nitroxide as it diffuses and dilutes into the deeper skin layers after penetration from the surface. A diagrammatic sketch of the nitroxide penetration and the clearance process that occur across the skin depth is illustrated in Fig. 4. The layer at the top of the skin is enriched with concentrated nitroxide. The amount of nitroxide in this layer is represented as M_1. Below this layer, there is a much thicker layer distributed with diluted nitrox-

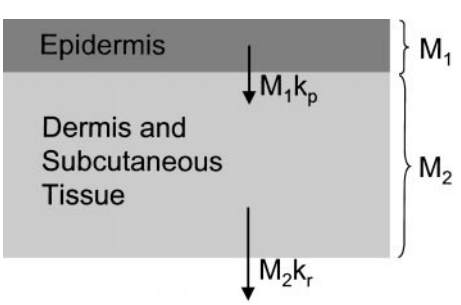

FIG. 4. Pharmacokinetic model of nitroxide distribution in the skin. The model assumes a nitroxide concentration, M_1, and a penetration rate constant, k_p, in the surface (epidermal) layer and a nitroxide concentration, M_2, and a clearance rate constant, k_r, in the deeper (dermis and subcutaneous) region of the skin. The clearance may include metabolic conversion of the nitroxide to EPR-silent forms and washout by perfusion.

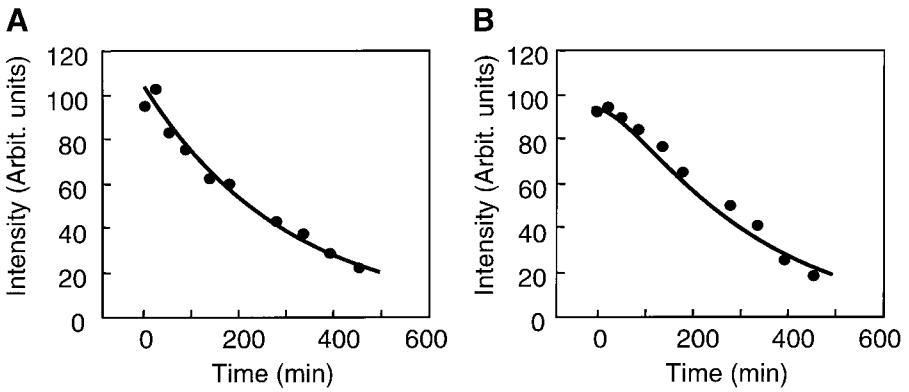

FIG. 5. Time course of nitroxide penetration and clearance in the skin of a human volunteer measured by *in vivo* topical EPR spectroscopy. The points represent (A) intensity of the central broad peak and (B) intensity of the whole spectrum, which includes the broad peak and the doublet components. The solid lines are theoretical fits using the kinetic model described in the text (Eqs. [1]–[5]). The fitting gave rate constants of 3.3×10^{-3} min^{-1} for penetration and 16.4×10^{-3} min^{-1} for clearance of nitroxide in the skin.

ide labels. The amount of nitroxide in the thicker layer is represented as M_2. The overall kinetic process is assumed to involve two major processes: the first process is the penetration of the nitroxide and the second process is the clearance of the nitroxide. The penetration process is assumed to be pseudo first order and its rate constant is defined as k_p such that the amount of radical penetrated into the skin in a unit time is $M_1 k_p$. When the radicals are inside the skin, there are two clearance processes that may occur. One is the reduction of the nitroxide to nonparamagnetic (EPR-inactive) forms that may occur due to enzymatic and/or chemical reduction by the reducing equivalents in the skin. The other is vascular washout, which may physically remove the nitroxide molecules from the active volume of the resonator. We use an overall rate constant k_r to represent these two processes, so that the total amount of the radicals that is cleared in a unit time is $M_2 k_r$. We further suppose that both the penetration and the clearance processes can be described by a single exponential function. If M_0 is the total amount of nitroxide that was initially applied to the skin, we can write the rate equations as

$$\begin{cases} \dfrac{dM_1}{dt} = -k_p M_1, & M_1|_{t=0} = M_0; \quad [1] \\ \dfrac{dM_2}{dt} = -\dfrac{dM_1}{dt} - k_r M_2, & M_2|_{t=0} = 0. \quad [2] \end{cases}$$

The solution to the above differential equations is

$$\begin{cases} M_1 = M_0 e^{-k_p t}; & [3] \\ M_2 = \dfrac{k_p M_0}{k_r - k_p} (e^{-k_p t} - e^{-k_r t}); & [4] \end{cases}$$

$$M_1 + M_2 = \frac{M_0 k_r}{k_r - k_p} e^{-k_p t} - \frac{M_0 k_p}{k_r - k_p} e^{-k_r t}. \quad [5]$$

In order to obtain the penetration rate constant k_p we used a fitting procedure of the time course of the integrated intensity of the middle broad peak. The data was fitted to Eq. [3] to obtain the rate constant k_p. The intensity data and the best fit are shown in Fig. 5A. A penetration rate constant of 3.29×10^{-3} min^{-1} was obtained from the data of this subject. As seen in Fig. 5A, the exponential decay function of Eq. [3] provided a reasonably good fit to the experimental data points.

The clearance rate constant k_r was obtained from the integrated intensity of the whole spectrum. The time dependence of the intensity is shown as the solid data points in Fig. 5B. We fitted the experimental data points using Eq. [5]. The best fit is shown as the solid line in the figure. From this fitting, we obtained the clearance rate constant of this subject as 16.4×10^{-3} min^{-1}.

We performed similar measurements of the nitroxide pharmacokinetics in the skin of a series of four normal human volunteers. Two of the volunteers were chosen to repeat the experiment 3 days later to check the reproducibility. The kinetic results are shown as bar graphs in Figs. 6A and 6B. Figure 6A shows the nitroxide penetration rate constants and Fig. 6B shows the clearance rate constant of the volunteers. The bars marked with asterisks are the repeated experimental data from the corresponding volunteers. From these two figures, we can see that while the rate constants are quite variable from person to person, in repeated experiments the results are very consistent in the same individual.

Skin Blood Flow Measurement

The clearance of the applied nitroxide radicals in biological systems can occur through bioreduction or vascular washout (*2*). While with topical application of the nitroxide label to the skin surface vascular washout would be greatly limited compared to that in other tissues, as the label penetrates into deeper layers of the skin this vascular clearance might significantly contribute to the clearance. Therefore, we performed experiments to measure the microvascular flow of the skin. In our experiment setup, we attached a specially designed holder to

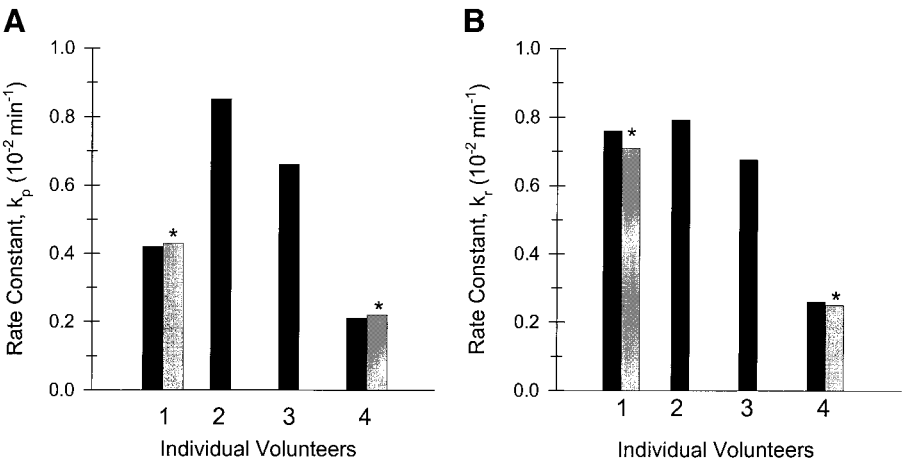

FIG. 6. Penetration and clearance rate constants for the nitroxide in the skin of human volunteers. The rate constants of penetration, A, and clearance, B, were measured from the normal human volunteers (1–4) as described in the text and shown in Fig. 5. *Data from repeat measurements on the same volunteer 3 days later. While prominent differences were observed among the individuals, data from the same individuals show good reproducibility.

the skin which was taped to the forearm with the volunteer's forearm resting on top of the resonator by it's own weight. In this situation, the microvascular blood flow of the covered skin could be markedly restricted. If so, then bioreduction would be the only significant clearance process.

Skin microvascular blood flow was measured using a laser Doppler detector (floLAB Laser Doppler blood flow monitor, Moor Instruments Limited, England) with a MP2 probe of 30-mm length and 6-mm diameter. The same type of skin holder was used and a hole was drilled at the bottom and then the probe was fixed to the bottom so that when the holder was attached to the skin, the surface of the probe is in contact with the skin surface. To measure baseline normal flow, the probe was carefully set to touch the skin surface with no mechanical pressure against the surface of the skin. After taping the EPR positioning spacer to the wrist, the flow was decreased by >85%. After the applied pressure of the weight of the wrist resting on the resonator, the blood flow was decreased by >90% from the baseline value. Thus, the localized microvascular flow of the skin within the positioning spacer was largely abolished. Therefore, the observed clearance of the nitroxide inside the skin would be expected to be primarily due to the metabolic bioreduction. This may explain why the observed clearance corresponded to a single exponential decay process.

Depth Profiling by 1-D Spatial Imaging

The depth profiling of the nitroxide deposited on the surface of the skin was investigated using 1-D spatial EPR imaging. A field gradient of 50 G/cm was applied normal to the surface. The low-field peak of the nitroxide doublet spectrum was used as the imaging component. This ensures that only the amount of label that penetrated inside the skin layers is imaged. In general, we utilize the low-field peak rather than the high-field peak in order to be able to apply our hyperfine correction algorithms (*25*). The 1-D spatial profile and the 1-D spatial color-coded image of the distribution of ^{15}N-PDT in the skin are illustrated in Figs. 7 and 8. The image shows two discrete bands of maximum intensity. The top band is located over the outer 400 μm of the skin where the epidermal layer is present. The second band is centered about 1000 μm from the surface

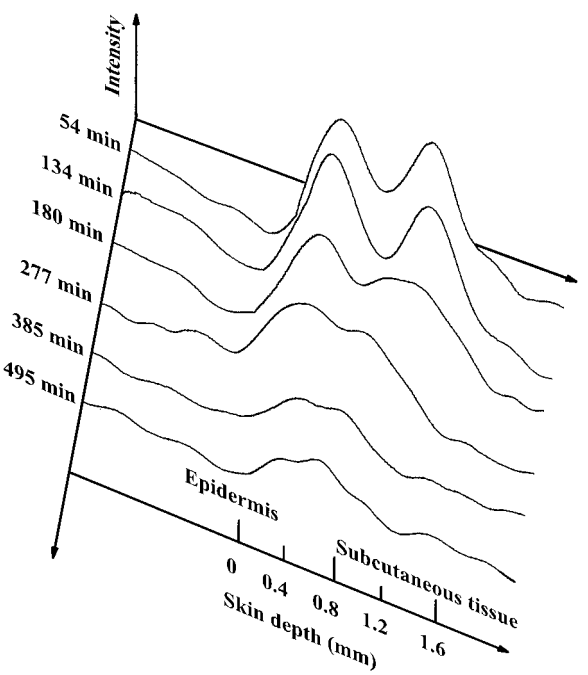

FIG. 7. Imaging of the time course of nitroxide distribution as a function of skin depth in human volunteers. A total of 3.5 μL of 100 mM ^{15}N-PDT was applied to the skin and 1-D EPR imaging of the distribution of the nitroxide along the direction perpendicular to the skin surface was performed. The profiles shown were obtained from the low-field line of the doublet ^{15}N-PDT signal by deconvolution of projections measured in the presence and absence of a 50 G/cm field gradient normal to the surface.

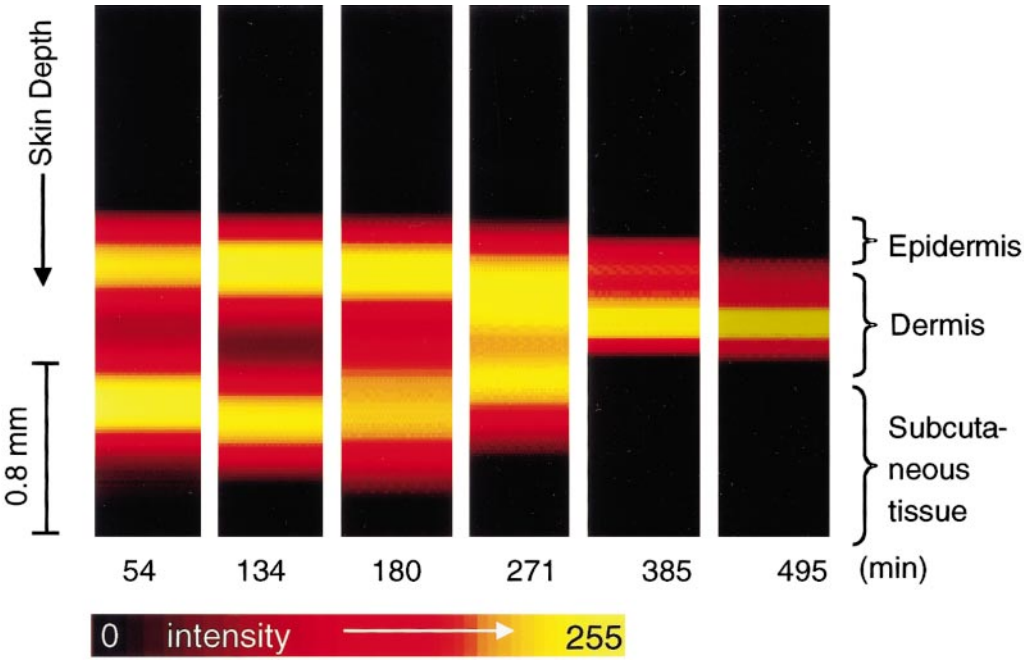

FIG. 8. Color-coded image of the time course of spatial distribution of the nitroxide as a function of skin depth. This image was obtained from the spatial profiles shown in Fig. 7. Two bands in the distribution of the label along the skin depth are seen. The first band appears in the outer 400 μm of the skin, the epidermis region, whereas the second band is centered at a depth of 1000 μm in the subcutaneous region with a thickness about 400 μm. These two bands decay and merge into a single band with time.

at the level of the subcutaneous tissue with a thickness of 400 μm. The distribution of the label changes with time at different depths (Figs. 7 and 8). After 8 h, the distribution merged into one central band centered about 500 μm from the surface.

Lateral Profiling by 2-D Spatial Imaging

To obtain the time course of the distribution of the label in the plane parallel to the skin surface, 2-D spatial imaging experiments were also performed on the nitroxide-treated skin of the human volunteers. A circular area of 20-mm diameter was imaged using a set of 16 projections per image obtained for every 15 s. A field gradient of 10 G/cm was used to resolve the spatial distribution of the label. The 2-D spatial images obtained from an individual volunteer are shown in Fig. 9. The time course images show that the intensity of the image (the amount of the label) inside the skin first increased and then decreased. This is consistent with the proposed kinetic model where the amount of the label in the skin is considered an intermediate controlled by two opposing exponential processes (penetration and clearance). The extension of the distribution

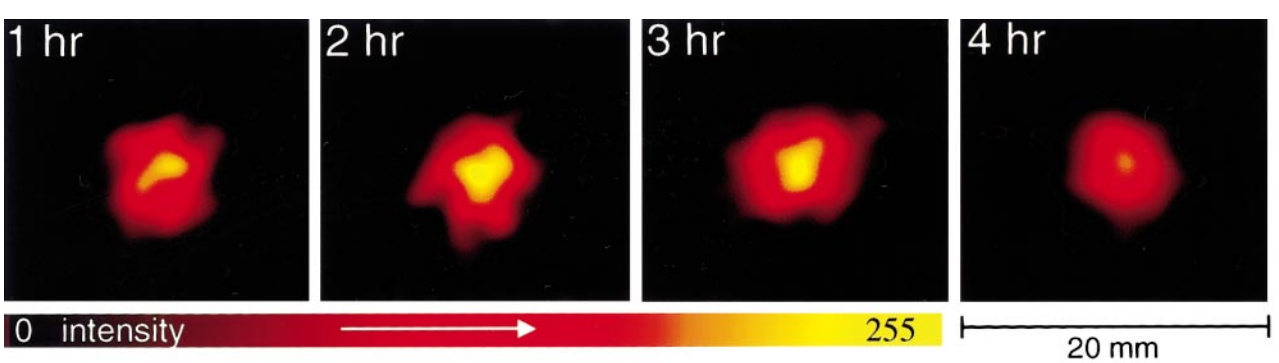

FIG. 9. Color-coded 2-D spatial image showing the time course of the nitroxide distribution along the plane of the skin surface. These images were obtained from the same human subject and experimental series shown in Figs. 7 and 8. The acquisition of these 2-D images along the skin surface was interspersed between that of the 1-D images perpendicular to the skin surface. The imaging was performed in the plane of the skin using a field gradient of 10 G/cm. Deconvolution of the zero gradient spectrum was performed. The distribution of the nitroxide in the skin at 1, 2, 3, and 4 h after the application of 3.5 μL of 100 mM ^{15}N-PDT is shown. Image acquisition parameters are as described in the text.

of the radicals along the skin surface is about 6 mm in diameter. This was exactly the area over which we applied the label on the surface of the skin and confirms that the label remained within the sensitive area of the surface resonator.

DISCUSSION

The major goal of our studies was to develop instrumentation and methodologies to be able to noninvasively measure and image the distribution and clearance of nitroxide radical spin labels in the skin of normal human volunteers. While there have been extensive prior studies measuring and imaging nitroxide free radicals and spin labels in isolated cultured cells and in skin biopsies (*10, 11, 15, 16–20*), no prior group has reported the successful imaging of nitroxides or other free radicals in *in vivo* skin. In the prior studies, important pioneering work was performed by Herrling *et al.* (*11*), who were the first to apply nitroxide labels to human skin. They performed surface EPR spectroscopy at S-band and measured the kinetics of clearance of millimolar concentrations of nitroxide labels applied to the skin (*11*). However, as they reported, they could not achieve sufficient sensitivity for *in vivo* imaging of free radicals in human skin. They did, however, report interesting studies imaging the distribution of nitroxide free radicals in skin biopsies (*11*).

In their *in vivo* human studies, Herrling *et al.* applied 10 μl of 1 mM TEMPO and TEMPOL in an emulsion vehicle to the skin with 4 min of incubation (*11*). After that, they used isotonic sodium chloride to wash off the skin and performed *in vivo* EPR spectroscopy measurements. As a comparison, we used 3.5 μl of 100 mM ^{15}N-PDT solution in aqueous vehicle (water) applied to the skin surface resulting in a small defined 2.5-mm spot of nitroxide on the skin surface. After 5 min without washing the surface of the skin, the positioner was attached to precisely fix the skin position and largely isolate the measured skin surface from vascular perfusion and EPR measurements were performed. Our protocol fixed the number of applied nitroxide molecules radicals left on the skin and greatly limited skin vascular flow, in principal leaving bioreduction as the major source of nitroxide clearance. In addition, the use of a high initial concentration of nitroxide where spin exchange occurs enabled measurement and modeling of the process of label diffusion and permeation in the skin as well as the process of clearance.

In preliminary experiments, we observed that when low millimolar concentrations of nitroxide labels such as tempone in aqueous vehicle were applied to the skin surface, the signal rapidly disappeared typically in less than 10 min. With imaging, it was seen that the nitroxide did not penetrate the skin surface with an observed depth of less than 0.1 mm. However, with concentrations in the range of 50 to 100 mM, persistent signal and penetration of the label within the skin were seen. When tempone was applied in a lipid vehicle such as olive oil or in water olive oil emulsions, it was observed to remain at the skin surface for long periods of time with little if any skin penetration. Therefore, in our studies where the main goal was to image the penetration of the nitroxide into the skin, we chose to use 100 mM concentrations of tempone in aqueous vehicle. In contrast to the earlier studies where the nitroxide was applied to the skin, allowed to adsorb for a time, and then wiped away with isotonic saline, we chose to apply a fixed amount of nitroxide to the skin and to allow this to be completely adsorbed so that the number of applied nitroxide molecules would not be altered by differences in skin absorbance or permeability and would be constant in all studies. In addition, the skin positioning piece served the double purpose of precisely fixing the skin for imaging and limiting microvascular flow, enabling bioreduction to be the major source of radical clearance. Thus, with our measurement protocol we were able to obtain information regarding the permeation and penetration of the label into the skin as well as its metabolic clearance. In addition, this protocol enabled the performance of *in vivo* EPR imaging of the spatial distribution of the nitroxide in human skin with well-resolved images of the radical distribution.

Another difference in our approach from that used in the earlier studies is with regard to the method used for spectral quantitation and analysis for the measurement of nitroxide clearance. In our experiments, we observed that the EPR lineshape of the spectral components of the nitroxide label applied to the skin changes over time. This is especially true when high concentrations of nitroxide are applied to the skin such that spin–spin exchange occurs. In addition, however, this was also a concern with lower nitroxide concentrations since the lineshape of the diluted nitroxide spectrum within the skin also changes over time. Therefore, we performed all spectral quantitation and kinetic analysis by integration of the whole EPR absorption function with fitting of individual spectral components. This is in contrast to the prior studies that used the signal intensity of only one peak to measure the reduction rate (*11*).

It is interesting that the clearance rate of the signal is much slower when higher concentrations of the label are used, such that penetration of the nitroxide into deeper skin layers occurs. It is possible that there may be a given concentration of ascorbate or other reducing equivalents that rapidly chemically react with the nitroxide at the skin surface, and that once the level of nitroxide exceeds the level of these reducing equivalents, skin penetration occurs. This might be accompanied by a much slower clearance process occurring due to other mechanisms such as cellular reduction by the mitochondrial respiratory enzymes or cellular processes. Indeed, it has been reported that the *in vivo* metabolism of nitroxides is largely governed by cellular reduction (*26*). Overall, it is clear that further studies will have to be performed in the future to better understand the chemical and cellular processes of *in vivo* nitroxide metabolism in the skin. Studies in both human subjects and animal models

will be of critical importance to resolve these important questions.

The properties of the skin including its permeability and redox metabolism could vary in different human individuals. This could be due to differences in diet, skin care, and sun exposure, as well as genetic or other factors. Indeed, we observed in the skin of a series of normal human volunteers that while the rate of nitroxide penetration and clearance was quite reproducible in a given individual, it was highly variable from person to person. Differences in the penetration rate constant of greater than two-fold were seen, as well as differences of more than four-fold in the clearance rate constant (Figs. 5 and 6). The images of nitroxide distribution in the skin of all subjects studied showed a characteristic pattern of two high-intensity bands with a region of low intensity in between. The first band appeared in the outer 400 μm of the skin, corresponding to the epidermal region, whereas the second band also had a thickness of about 400 μm and was centered at a depth of 1000 μm, corresponding to the location of subcutaneous tissue beneath the dermis. The central region of low intensity occurred at a depth corresponding to the dermis. These studies suggest that the dermis has either a higher concentration of reducing equivalents or a greater capability for cellular nitroxide reduction than the deeper subcutaneous tissue. Future studies will be need to characterize the chemical and cellular basis for the interindividual differences in the skin permeability and metabolism as well as the differences in radical metabolism seen in the layers of the skin.

SUMMARY AND CONCLUSIONS

Instrumentation and methods were developed that enabled the first *in vivo* imaging of free radicals in human subjects with the use of nitroxide spin labels. Pharmacokinetic and spatial mapping of the distribution of a nitroxide label applied to human skin were measured *in vivo* using S-band topical EPR imaging instrumentation with a specially designed surface resonator. Noninvasive studies of the distribution and redox metabolism of a topically applied nitroxide label (^{15}N-PDT) in the skin were performed. The penetration process from the skin surface into the dermis and subcutaneous regions and the clearance process from these regions were described by single exponential functions. The imaging measurements in the skin showed two bands in the distribution of the label along the skin depth. The first band appeared in the outer 400 μm of the skin, the epidermis region, whereas the second band was centered at a depth of 1000 μm in the subcutaneous region with a thickness of about 400 μm. These two bands decayed and merged into a single weaker band with time. The experiments also demonstrate that EPR spectroscopy and imaging enable noninvasive detection and mapping of free radicals in the skin. This technique can provide important data regarding redox state and free radical metabolism in the skin and thus has great promise in the study of dermatological disease and development of skin treatment formulations.

ACKNOWLEDGMENTS

We are grateful to Michael Chzhan for his technical help in the construction of the resonator and the volunteers for their time and cooperation. This work was supported by NIH Grants RR 12190, GM58582, and CA 78886 and the Unilever Corporation.

REFERENCES

1. L. J. Berliner and H. Fujii, Magnetic resonance imaging of biological specimens by electron paramagnetic resonance of nitroxide spin labels, *Science* **227,** 517–519 (1985).
2. J. L. Zweier and P. Kuppusamy, Electron paramagnetic resonance measurements of free radicals in the intact beating heart: A technique for detection and characterization of free radicals in whole biological tissues, *Proc. Natl. Acad. Sci. USA* **85,** 5703–5707 (1988).
3. H. J. Halpern, D. P. Spencer, J. V. Polen, M. K. Bowman, A. C. Nelson, E. M. Dowey, and B. A. Teicher, Imaging radio frequency electron spin resonance spectrometer with high resolution and sensitivity for *in vivo* measurements, *Rev. Sci. Instrum.* **60,** 1040–1050 (1989).
4. K. Chen, C Ng, J. L. Zweier, J. D. Glickson, and H. M. Swartz, Measurement of the intracellular concentration of oxygen in a cell perfusion system, *Magn. Reson. Med.* **31,** 668–672 (1994).
5. P. Kuppusamy and J. L. Zweier, Evaluation of nitroxides for the study of myocardial metabolism and oxygenation, *Magn. Reson. Chem.* **33,** S123–S128 (1995).
6. P. Kuppusamy, M. Chzhan, K. Vij, M. Shteynbuk, E. Gianella, D. J. Lefer, and J. L. Zweier, 3-Dimensional spectral spatial EPR imaging of free radicals in the heart. A technique for imaging tissue metabolism and oxygenation, *Proc. Natl. Acad. Sci. USA* **91,** 3388–3392 (1994).
7. P. Kuppusamy, M. Chzhan, and J. L. Zweier, Development and optimization of three dimensional spatial EPR imaging for biological organs and tissues, *J. Magn. Reson. B* **106,** 122–130 (1995).
8. P. Kuppusamy, P. Wang, and J. L. Zweier, Three-dimensional spatial EPR imaging of the rat heart, *Magn. Reson. Med.* **34,** 99–105 (1995).
9. P. Kuppusamy, R. A. Shankar, and J. L. Zweier, *In vivo* measurement of arterial and venous oxygenation in the rat using 3D spectral–spatial electron paramagnetic resonance imaging, *Phys. Med. Biol.* **43,** 1837–1844 (1998).
10. J. Fuchs, N. K. Groth, T. E. Herrling, and G. Zimmer, Electron paramagnetic resonance studies on nitroxide radical 2,2,5,5-tetramethyl-4-piperidin-1-oxyl (TEMPO) redox reactions in human skin, *Free Rad. Biol. Med.* **22,** 967–976 (1997).
11. T. E. Herrling, N. K. Groth, and J. Fuchs, Biochemical EPR imaging of skin, *Appl. Magn. Reson.* **11,** 471–486 (1996).
12. J.-L. Leveque and P. G. Agache, "Aging Skin: Properties and Functional Changes," Dekker, New York, 1993.
13. K. Mader, G. Bacic, and H. M. Swartz, *In-vivo* detection of anthralin-derived free radicals in the skin of hairless mice by low-frequency electron paramagnetic-resonance spectroscopy, *J. Invest. Dermatol.* **104,** 514–517 (1995).
14. C. Michel, N. Groth, T. Herrling, P. Rudolph, J. Fuchs, J. Kreuter,

and H. J. Freisleben, Penetration of spin-labeled retinoic acid from liposomal preparations into the skin of SKH1 hairless mice measurement by EPR tomography, *Int. J. Pharmaceut.* **98,** 131–139 (1993).

15. J. Fuchs, N. Groth, T. E. Herrling, R. Milbradt, G. Zimmer, and L. Packer, Electron paramagnetic resonance (EPR) imaging in skin biophysical and biochemical microscopy, *J. Invest. Dermatol.* **98,** 713–719 (1992).
16. B. A. Jurkiewicz and G. R. Buettner, EPR detection of free radicals in UV-irradiated skin: Mouse versus human, *Photochem. Photobiol.* **64,** 918–922 (1996).
17. B. Collins, T. O. Poehler, and W. A. Bryden, EPR persistence measurements of UV-induced melanin free radicals in whole skin, *Photochem. Photobiol.* **62,** 557–560 (1995).
18. B. A. Jurkiewicz and G. R. Buettner, Ultraviolet light-induced free radical formation in skin an electron paramagnetic resonance study, *Photochem. Photobiol.* **59,** 1–4 (1994).
19. C. M. Arroyo and S. J. Janny, EPR spin-label technique as an analytical tool for determining the resistance of reactive topical skin protectants (RTSPS) to the breakthrough of vesicant agents, *J. Pharmacol. Toxicol. Methods* **33,** 109–112 (1995).
20. V. Gabrijelcic, M. Sentjurc, and M. Schara, The measurement of liposome-entrapped molecules penetration into the skin A 1D-EPR and EPR kinetic imaging study, *Int. J. Pharmaceut.* **102,** 151–158 (1994).
21. G. He, R. A. Shankar, M. Chzhan, A. Samouilov, P. Kuppusamy, and J. L. Zweier, Noninvasive measurement of anatomic structure and intraluminal oxygenation on the gastrointestinal tract of living mice with spatial and spectral EPR imaging, *Proc. Natl. Acad. Sci. USA* **96,** 4586–4591 (1999).
22. P. Kuppusamy, M. Chzhan, A. Samouilov, P. Wang, and J. L. Zweier, Mapping the spin-density and lineshape distribution of free radicals using 4D spectral–spatial EPR imaging, *J. Magn. Reson. B* **107,** 116–125 (1995).
23. L. J. Berliner and J. Reuben, "Biological Magnetic Resonance: Spin Labeling-Theory and Applications," Plenum Press, New York, 1989.
24. J. -H. Sachse and D. Marsh, Line intensities in spin-exchanged nitroxide ESR spectra, *J. Magn. Reson.* **68,** 540–543 (1986).
25. P. Kuppusamy and J. L. Zweier, A forward subtraction procedure for removing hyperfine artifacts in electron paramagnetic resonance imaging, *Magn. Reson. Med.* **35,** 316–322 (1996).
26. H. M. Swartz, in "Advances in Magnetic Resonance Imaging" (E. Feig, Ed.), pp. 49–71, Ablex Publishing, Norwood, NJ.